AIP | Journal of Applied Physics

Thermal properties of microscale inorganic light-emitting diodes in a pulsed operation

Yuhang Li, Yan Shi, Jizhou Song, Chaofeng Lu, Tae-il Kim et al.

Citation: J. Appl. Phys. **113**, 144505 (2013); doi: 10.1063/1.4800858
View online: http://dx.doi.org/10.1063/1.4800858
View Table of Contents: http://jap.aip.org/resource/1/JAPIAU/v113/i14
Published by the American Institute of Physics.

Thermal properties of microscale inorganic light-emitting diodes in a pulsed operation

Yuhang Li,[1,2,a)] Yan Shi,[1,3,a)] Jizhou Song,[4,b)] Chaofeng Lu,[5] Tae-il Kim,[6,7] John A. Rogers,[6] and Yonggang Huang[1,b)]
[1]*Department of Civil and Environmental Engineering and Department of Mechanical Engineering, Northwestern University, Evanston, Illinois 60208, USA*
[2]*Department of Engineering Mechanics, Zhejiang University, Hangzhou 310027, China*
[3]*State Key Laboratory of Mechanics and Control of Mechanical Structures, Nanjing University of Aeronautics and Astronautics, Nanjing 210016, China*
[4]*Department of Mechanical and Aerospace Engineering, University of Miami, Coral Gables, Florida 33146, USA*
[5]*Department of Civil Engineering and Soft Matter Research Center, Zhejiang University, Hangzhou 310058, China*
[6]*Department of Materials Science and Engineering, Frederick Seitz Materials Research Laboratory, University of Illinois at Urbana-Champaign, Urbana, Illinois 61801, USA*
[7]*School of Chemical Engineering, Sungkyunkwan University (SKKU), Suwon 440-746, Korea*

(Received 1 February 2013; accepted 25 March 2013; published online 10 April 2013)

Light-emitting diodes (LEDs) in a pulsed operation offer combined characteristics in efficiency, thermal management, and communication, which make them attractive for many applications such as backlight unit, optical communication, and optogenetics. In this paper, an analytic model, validated by three dimensional finite element analysis and experiments, is developed to study the thermal properties of micro-scale inorganic LEDs (μ-ILED) in a pulsed operation. A simple scaling law for the μ-ILED temperature after saturation is established in terms of the material and geometrical parameters of μ-ILED systems, peak power, and duty cycle. It shows that the normalized maximum temperature increase only depends on two non-dimensional parameters: normalized μ-ILED area and duty cycle. This study provides design guidelines for minimizing adverse thermal effects of μ-ILEDs.
 [http://dx.doi.org/10.1063/1.4800858]

I. INTRODUCTION

Inorganic light-emitting diodes (LEDs) are attractive for broad classes of applications in solid state lighting due to their high efficiency and lifetime.[1,2] Many other applications such as backlight unit and optical communications require LEDs to be operated by pulsed current (or power) to take advantage of their high efficiency, thermal management, and effective application in communication.[3,4] Pulsed mode can provide additional benefits, especially in applications of optogenetics, where the biological response can be suppressed by the continuous mode operation.[5]

Recently, Kim *et al*. reported strategies to enable efficient, ultrathin micro-scale inorganic LEDs (μ-ILEDs), and their integration onto unconventional substrates such as hydrogel to simulate biological tissue.[3] The process began with high quality epitaxial material grown using state-of-the art techniques on sapphire substrates followed by the definition of the size of individual μ-ILED ($\sim 100\,\mu\text{m} \times 100\,\mu\text{m}$). The technique of transfer printing was used to release the completed μ-ILED onto the hydrogel substrate with a polyimide (PI) layer on the top to ensure a good contact between μ-ILED and the substrate. A photo-definable layer of epoxy (SU8) encapsulated the device but left the p- and n-type contacts (yellow part in Fig. 1(a)) exposed. Two electrodes were then used to provide pulsed power to drive the μ-ILED in order to study its thermal behaviors. Optical measurements of the emission spectra and light output were performed with a spectrometer (HR4000 and FOIS-1 fiber optics integrating sphere, Ocean Optics). Radiant efficiency to be used to calculate the power for μ-ILED was simply obtained from the light output power divided by the input electrical power. The SU8 surface temperature, measured by a QFI Infra-Scope Micro-Thermal Imager, was approximately the same as the μ-ILED temperature because the SU8 layer directly above the μ-ILED was very thin ($\sim 0.5\,\mu\text{m}$). Figure 1(a) shows the layouts of a single μ-ILED on a PI layer attaching to a hydrogel substrate encapsulated by a SU8 layer, and the cross section is shown in Fig. 1(b). The pulsed power applied to the μ-ILED is denoted by $Q(t) = Q_0 U(t)$ with Q_0 as the peak power and $U(t)$ as a unit pulsed power as shown in Fig. 1(c). The duty cycle is defined as $D = \tau/t_0$, where τ is the pulse duration and t_0 is the period of the pulse. The brightness can be controlled by adjusting the pulse duty cycle D without changing the color characteristics of LEDs.

The thermal properties of μ-ILED devices are critically important because excessive heating can limit the stability, reliability, and efficiency. Thermal studies of μ-ILEDs have been carried out for similar layouts as Fig. 1(a) in steady-state conditions with a continuous direct current (or power) input.[3,6,7] For μ-ILEDs with a pulsed current (or power), Kim *et al*. performed a three-dimensional (3D) finite element analysis (FEA) to investigate the thermal properties of the μ-ILED (Fig. 1(a)).[3] As shown in Fig. 1(d) for the pulsed peak power $Q_0 = 30$ mW with duty cycle $D = 50\%$ and period $t_0 = 1.0$ ms, the μ-ILED temperature increased, at first, in a fluctuation way, then reached saturation in a band after a few seconds, and the band did not change with the operating time.[8] The maximum

[a)]Y. Li and Y. Shi contributed equally to this work.
[b)]Authors to whom correspondence should be addressed. Electronic addresses: jsong8@miami.edu and y-huang@northwestern.edu

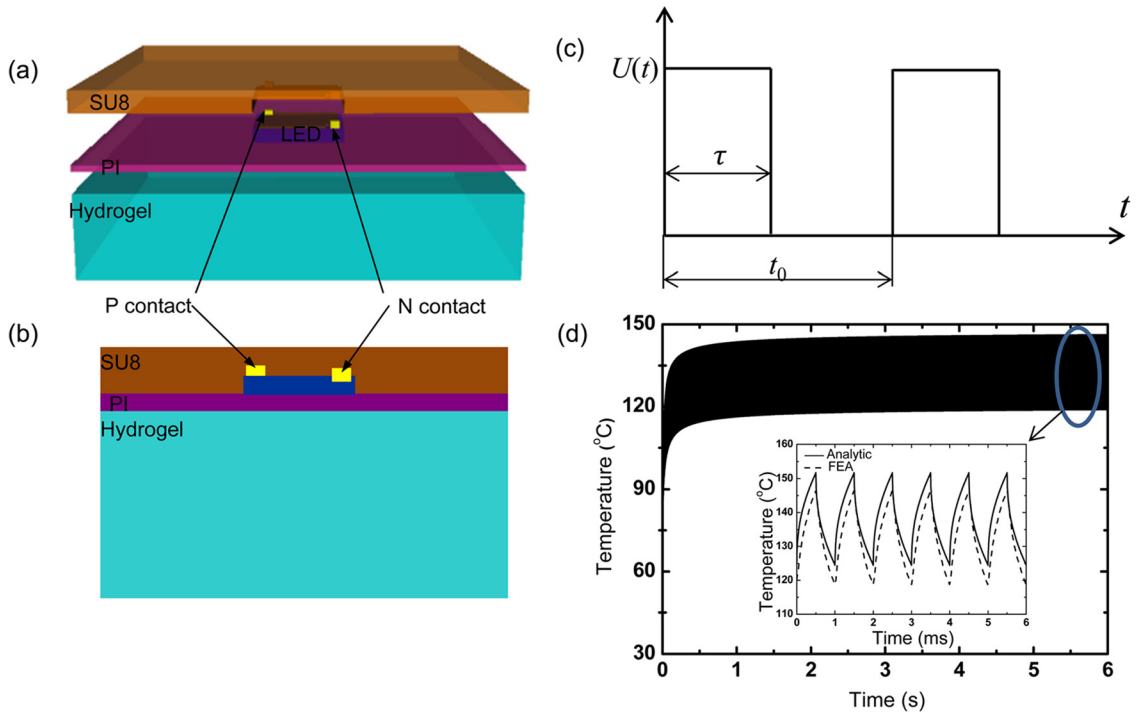

FIG. 1. (a) Three-dimensional and (b) cross-sectional illustrations of μ-ILED structure. (c) Unit pulsed power $U(t)$ with duration time τ and period t_0. (d) Temperature obtained from FEA for the pulsed peak power 30 mW with 50% duty cycle and period 1 ms with the inset showing the temperature by analytic model and FEA after saturation.

temperature, which determined the performance of μ-ILEDs, was reached after the saturation.

Several thermal models and approaches have been proposed to accurately and efficiently predict the LED temperature in a pulsed operation. Most of them are expressed as a thermal resistor-capacitor (RC) network,[8–12] which is solved by commercial or open programs such as FLOTHERM and SPICE. The RC network approach can save significant time and effort, but the values for R and C for different sections of LED packages need be determined from the curve-fitting of a transient thermal measurement of the package. Other methods such as multi-exponential method, finite volume method, and finite element method are also used to obtain the LED temperature.[13–17] However, none of them can give the LED temperature with pulsed power directly in terms of material properties, geometric, and loading parameters.

This paper aims at developing an analytic model, as validated by experiments and 3D FEA, to study the thermal properties of μ-ILED systems in a pulsed operation. A simple scaling law for the μ-ILED temperature after saturation is established analytically in terms of the material and geometrical parameters of μ-ILED systems, peak power, and duty cycle. The scaling law is very useful for the design and optimization of μ-ILED systems.

II. HEAT CONDUCTION MODEL FOR THE μ-ILED SYSTEM IN A PULSED OPERATION

As shown in Figs. 1(a) and 1(b), the μ-LED is on the PI/hydrogel substrate and is encapsulated by the SU8 layer. The thickness of the μ-LED, 6.54 μm, is much smaller than its in-plane size L (100 μm × 100 μm). Heat transfer mainly occurs through the top and bottom surfaces of μ-LED such that it can be modeled as a planar heat source at the SU8-PI interface. The thermal conductivity of 0.52 W/(m K) and thermal diffusivity of 3.2×10^{-7} m^2/s of the PI layer[18,19] are close to those of hydrogel [thermal conductivity 0.6 W/(m K) and thermal diffusivity 2.3×10^{-7} m^2/s][20,21] such that the PI layer and hydrogel substrate are modeled as a single hydrogel layer. Furthermore, the hydrogel substrate has a thickness (~2 mm) much larger than that of SU8 encapsulation (7 μm) and the thickness (6.54 μm) and in-plane size (100 μm) of μ-LED, and is therefore modeled as a semi-infinite substrate. For simplicity, an axisymmetric model is adopted where the heat source is modeled as a circular disk of $r_0 = L/\sqrt{\pi}$ such that it has the same area (L^2) of the μ-ILED. These assumptions, as validated by experiments and 3D FEA of square μ-ILED, significantly simplify the analysis to obtain the analytic solution.

Figure 2 shows a schematic illustration of the analytic model of a SU8 encapsulation layer with thickness h_{encap} on a semi-infinite hydrogel substrate subjected to a circular disk heat source $Q(t) = Q_0 U(t)$ with radius r_0 at the SU8/hydrogel interface. The origin of the cylindrical coordinate system (r,z) is at the center of heat source (Fig. 2). The temperature change from the ambient temperature, $\Delta T = T - T_\infty$, satisfies the heat conduction equation:

$$\frac{\partial \Delta T}{\partial t} - \alpha\left(\frac{\partial^2 \Delta T}{\partial r^2} + \frac{1}{r}\frac{\partial \Delta T}{\partial r} + \frac{\partial^2 \Delta T}{\partial z^2}\right) = 0, \qquad (1)$$

where $\alpha = k/(c\rho)$ is thermal diffusivity with k as thermal conductivity, c as specific heat capacity, and ρ as mass density. In the following, the subscripts *encap* and *sub* denote the encapsulation and substrate, respectively.

At the top surface of SU8 ($z = -h_{encap}$), natural convection has a negligible effect on the device temperature,[3] which gives

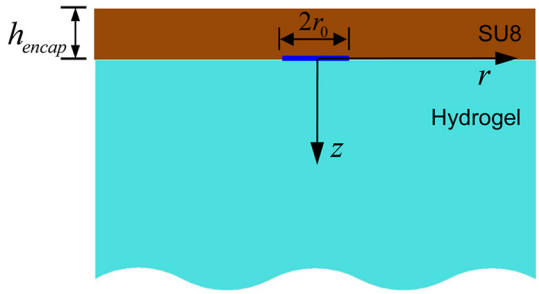

FIG. 2. A schematic illustration of the analytically modeled μ-LED system.

$$-k_{encap}\frac{\partial \Delta T}{\partial z}\bigg|_{z=-h_{encap}} = 0. \tag{2}$$

Across the SU8/hydrogel interface ($z = 0$), the temperature is continuous

$$\Delta T\big|_{z=0^+} = \Delta T\big|_{z=0^-}, \tag{3}$$

and the heat flux is also continuous except the region of heat source ($z = 0, r \le r_0$)

$$-k_{sub}\frac{\partial \Delta T}{\partial z}\bigg|_{z=0^+} + k_{encap}\frac{\partial \Delta T}{\partial z}\bigg|_{z=0^-} = \begin{cases} 0 & r > r_0 \\ \dfrac{Q(t)}{\pi r_0^2} & 0 \le r \le r_0 \end{cases}. \tag{4}$$

The ambient temperature at the bottom surface of hydrogel ($z = \infty$) gives

$$\Delta T\big|_{z=\infty} = 0. \tag{5}$$

The periodic pulsed power can be expressed via its Fourier series as

$$Q(t) = Q_0\begin{cases} 1 & 0 < t \le \tau \\ 0 & \tau < t \le t_0 \end{cases} = Q_0\left(a_0 + \sum_{n=1}^{\infty} a_n \cos n\omega t + \sum_{n=1}^{\infty} b_n \sin n\omega t\right), \tag{6}$$

where $\omega = 2\pi/t_0$, $a_0 = D = \tau/t_0$, $a_n = \sin(2n\pi D)/(n\pi)$, and $b_n = [1 - \cos(2n\pi D)]/(n\pi)$. In the following, we will first obtain the temperature increase due to a sinusoidal power $Q_0\cos(\omega t)$ [or $Q_0\sin(\omega t)$] and then use the method of superposition to obtain ΔT due to $Q(t)$.

A. Temperature increase due to a sinusoidal power

A sinusoidal power $Q_0\cos(\omega t)$ [or $Q_0\sin(\omega t)$] can be written as the real (or imaginary) part of $Q_0 e^{i\omega t}$. The temperature increase at saturation has the same frequency and takes the form $\theta(r, z; \omega)e^{i\omega t}$, where $\theta(r, z; \omega) = |\theta(r, z; \omega)|e^{i\beta}$, and the phase angle β is given by

$$\beta = \begin{cases} \arctan\left\{\dfrac{\mathrm{Im}[\theta(r,z;\omega)]}{\mathrm{Re}[\theta(r,z;\omega)]}\right\} & \mathrm{Re}[\theta(r,z;\omega)] > 0 \\ \arctan\left\{\dfrac{\mathrm{Im}[\theta(r,z;\omega)]}{\mathrm{Re}[\theta(r,z;\omega)]}\right\} + \pi & \mathrm{Re}[\theta(r,z;\omega)] < 0 \ \&\ \mathrm{Im}[\theta(r,z;\omega)] \ge 0 \\ \arctan\left\{\dfrac{\mathrm{Im}[\theta(r,z;\omega)]}{\mathrm{Re}[\theta(r,z;\omega)]}\right\} - \pi & \mathrm{Re}[\theta(r,z;\omega)] < 0 \ \&\ \mathrm{Im}[\theta(r,z;\omega)] < 0 \\ \dfrac{\pi}{2} & \mathrm{Re}[\theta(r,z;\omega)] = 0 \ \&\ \mathrm{Im}[\theta(r,z;\omega)] > 0 \\ -\dfrac{\pi}{2} & \mathrm{Re}[\theta(r,z;\omega)] = 0 \ \&\ \mathrm{Im}[\theta(r,z;\omega)] < 0 \end{cases} \tag{7}$$

Substitution of $\theta(r, z; \omega)e^{i\omega t}$ into Eq. (1) gives

$$\frac{\partial^2\theta}{\partial r^2} + \frac{1}{r}\frac{\partial\theta}{\partial r} + \frac{\partial^2\theta}{\partial z^2} - iq^2\theta = 0, \tag{8}$$

where $q = \sqrt{\omega/\alpha}$. The Hankel transform $\bar{\theta}(\xi, z; \omega) = \int_0^\infty \theta(r, z; \omega)J_0(\xi r)r\mathrm{d}r$, where J_0 is the 0th-order Bessel function of the first kind, then yields an ordinary differential equation:

$$\frac{d^2\bar{\theta}}{dz^2} - (\xi^2 + iq^2)\bar{\theta} = 0, \tag{9}$$

which has the solution

$$\bar{\theta} = A(\xi)e^{z\sqrt{\xi^2+iq^2}} + B(\xi)e^{-z\sqrt{\xi^2+iq^2}}, \tag{10}$$

where $A(\xi)$ and $B(\xi)$ are to be determined, and are denoted by A_{encap} and B_{encap} for the SU8 encapsulation, and A_{sub} and B_{sub} for the hydrogel substrate, respectively. The Hankel transform of boundary and continuity conditions in Eqs. (2)–(5) give these functions as

$$\begin{Bmatrix} A_{encap} \\ B_{encap} \\ A_{sub} \\ B_{sub} \end{Bmatrix} = \frac{Q_0}{2\pi r_0}f(\xi)\frac{J_1(\xi r_0)}{\xi}\begin{Bmatrix} e^{h_{encap}\sqrt{\xi^2+iq_{encap}^2}} \\ e^{-h_{encap}\sqrt{\xi^2+iq_{encap}^2}} \\ 0 \\ 2\cosh(h_{encap}\sqrt{\xi^2+iq_{encap}^2}) \end{Bmatrix}, \tag{11}$$

where J_1 is the 1st Bessel function of the first kind

$$f(\xi) = \frac{1}{k_{sub}\sqrt{\xi^2 + iq_{sub}^2}\cosh\left(h_{encap}\sqrt{\xi^2 + iq_{encap}^2}\right) + k_{encap}\sqrt{\xi^2 + iq_{encap}^2}\sinh\left(h_{encap}\sqrt{\xi^2 + iq_{encap}^2}\right)}, \tag{12}$$

$q_{encap} = \sqrt{\omega/\alpha_{encap}}$, and $q_{sub} = \sqrt{\omega/\alpha_{sub}}$.

The inverse Hankel transform $\theta(r,z;\omega) = \int_0^\infty \bar{\theta}(\xi,z;\omega) J_0(\xi r)\xi d\xi$ gives θ_{encap} and θ_{sub} in the SU8 encapsulation and hydrogel substrate as

$$\theta_{encap}(r,z;\omega) = \frac{Q_0}{\pi r_0}\int_0^\infty f(\xi)J_1(\xi r_0)J_0(\xi r) \times \cosh\left[(z + h_{encap})\sqrt{\xi^2 + iq_{encap}^2}\right]d\xi, \tag{13}$$

$$\theta_{sub}(r,z;\omega) = \frac{Q_0}{\pi r_0}\int_0^\infty f(\xi)J_1(\xi r_0)J_0(\xi r) \times \cosh\left(h_{encap}\sqrt{\xi^2 + iq_{encap}^2}\right)e^{-z\sqrt{\xi^2+iq_{sub}^2}}d\xi. \tag{14}$$

The temperature increase on the surface ($z = -h_{encap}$) of SU8 encapsulation, which is to be used in the comparison with 3D FEA in Sec. III, is given by

$$\theta_{surface}(r;\omega) = \frac{Q_0}{\pi r_0}\int_0^\infty f(\xi)J_1(\xi r_0)J_0(\xi r)d\xi. \tag{15}$$

The μ-ILED has much larger thermal conductivity [160 W/(m K)][22] than SU8 [0.20 W/(m K)],[23] PI [0.52 W/(m K)],[18] and hydrogel [0.60 W/(m K)].[20] Therefore, the temperature increase in μ-ILED is relatively uniform.[3,6,7] In addition, the uniform volumetric heat source of μ-ILED also helps its temperature to be uniform.[6] The μ-ILED temperature can be approximately by the average temperature of SU8/hydrogel interface over the entire region of μ-ILED ($z = 0$, $0 \le r \le r_0$)[7]

$$\theta_{LED}(\omega) = \frac{2Q_0}{\pi r_0^2}\int_0^\infty f(\xi)\frac{J_1{}^2(\xi r_0)}{\xi} \times \cosh\left(h_{encap}\sqrt{\xi^2 + iq_{encap}^2}\right)d\xi. \tag{16}$$

B. Temperature increase due to a pulsed power

For a pulsed power (Fig. 1(c)) given in Eq. (6), the temperature increase can be obtained by the superposition of solutions in Eqs. (13)–(16). In particular, the temperature increase on the surface of SU8 encapsulation is given by

$$\Delta T_{surface}(r,t;\omega) = D\theta_{surface}(r;0) + \sum_{n=1}^{\infty}|\theta_{surface}(r;n\omega)| \times \left[\frac{\sin(2n\pi D)}{n\pi}\cos(n\omega t + \beta_n) + \frac{1-\cos(2n\pi D)}{n\pi}\sin(n\omega t + \beta_n)\right], \tag{17}$$

where β_n is the phase angle of $\theta_{surface}(r;n\omega)$ as defined by Eq. (7). The temperature increase of μ-ILED is

$$\Delta T_{LED}(t;\omega) = D\theta_{LED}(0) + \sum_{n=1}^{\infty}|\theta_{LED}(n\omega)| \times \left[\frac{\sin(2n\pi D)}{n\pi}\cos(n\omega t + \gamma_n) + \frac{1-\cos(2n\pi D)}{n\pi}\sin(n\omega t + \gamma_n)\right], \tag{18}$$

where γ_n is the phase angle of $\theta_{LED}(n\omega)$.

The inset of Fig. 1(d) compares the μ-ILED temperature after saturation from Eq. (18) and the accurate 3D FEA for the pulsed peak power $Q_0 = 30$ mW with the duty cycle $D = 50\%$ and the period $t_0 = 1.0$ ms. The thermal conductivity, heat capacity, mass density, and layer thickness were 0.20 W/(m K), 1200 J/(kg K), 1190 kg/m^3, and 7 μm for SU8;[3,23] 160 W/(m K), 700 J/(kg K), 2329 kg/m^3, and 6.54 μm for μ-ILED;[22] 0.52 W/(m K), 1150 J/(kg K), 1430 kg/m^3, and 2 μm for PI;[18,19] and 0.6 W/(m K), 2375 J/(kg K), 1112 kg/m^3, and 2 mm for hydrogel,[20,21] respectively. The top surface of SU8 had natural convection with the coefficient of heat convection 25 W/(m^2 K) while the other surfaces were at a constant ambient temperature $T_\infty = 30\,^\circ$C. The continuum element DC3D8 in the ABAQUS software was used in FEA.[24] The temperature increases during the pulse duration and then decreases between pulses. The good agreement of temperature between analytic and FEA validates the assumptions used in the analytic model.

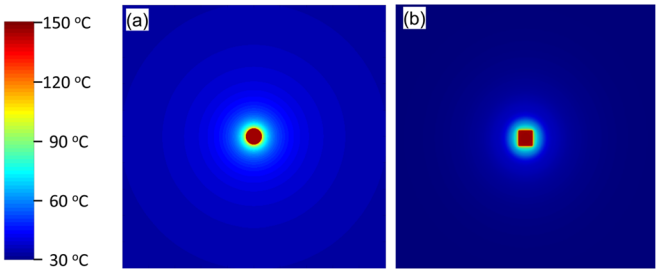

FIG. 3. Surface temperature distribution given by (a) analytic model and (b) FEA for the pulsed peak power 30 mW with 50% duty cycle and period 1 ms.

To further validate the analytic model, Fig. 3 compares the surface temperature distribution in Eq. (17), when ΔT_{LED} reaches the maximum, to that obtained by accurate 3D FEA at peak power $Q_0 = 30\,\text{mW}$ with the duty cycle $D = 50\%$ and the period $t_0 = 1.0\,\text{ms}$. The analytic model agrees reasonably well with the FEA. This is further validated by the maximum and minimum temperature increases of μ-ILED for various duty cycles at 30 mW, together with the experimentally measured temperature of μ-ILED, all shown in Fig. 4. The analytic model and FEA agree well, and the experimental data are indeed within the maximum and minimum temperature increase given by the analytic model. For duty cycle D decreasing from 100% (i.e., constant power) to 1%, ΔT_{LED} decreases from $\sim$202 °C to $\sim$0.5 °C, which suggests that μ-ILEDs can be operated in a pulsed mode at a high power density but a low temperature increase. This is important for applications to optogenetics, which require the peak power density of $\sim$10 mW/mm^2 with sustained temperature increase less than 1–2 °C.[5] At this peak, power density of 10 mW/mm^2, the present design of μ-ILEDs in Fig. 1 gives the maximum temperature increase only $\sim$0.4 °C at 50% duty cycle, and 0.1 °C at 10% duty cycle.

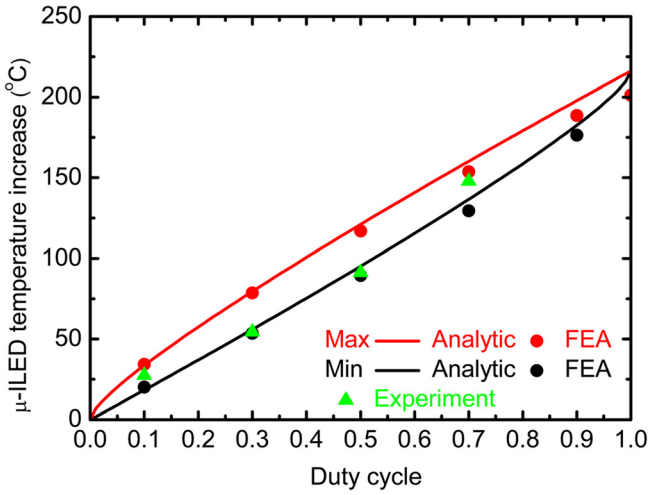

FIG. 4. The μ-ILED temperature increase versus duty cycle for the peak power 30 mW with period 1 ms.

III. A SCALING LAW FOR μ-ILED TEMPERATURE IN A PULSED OPERATION

The temperature increase of μ-ILED in a pulsed operation given in Eq. (18) is rather complex. A simple scaling law is established in this section, which clearly shows the influences of various material, geometric, and loading (heating) parameters, and is useful to optimize the design of μ-ILED.

A. A scaling law for temperature increase due to a sinusoidal power

Equation (16) can be rewritten by the change of integration variable $\eta = \xi r_0$ as

$$\theta_{LED}(\omega) = \frac{2Q_0}{\pi k_{sub} r_0} \int_0^\infty \left\langle \left\{ 1 + \frac{k_{encap}}{k_{sub}} \frac{\sqrt{\eta^2 + \mathrm{i}(r_0^2\omega/\alpha_{encap})}}{\sqrt{\eta^2 + \mathrm{i}(r_0^2\omega/\alpha_{sub})}} \tanh\left[\frac{h_{encap}}{r_0} \sqrt{\eta^2 + \mathrm{i}(r_0^2\omega/\alpha_{encap})} \right] \right\}^{-1} \cdot \frac{{J_1}^2(\eta)}{\eta\sqrt{\eta^2 + \mathrm{i}(r_0^2\omega/\alpha_{sub})}} \right\rangle \mathrm{d}\eta. \tag{19}$$

The last term $\frac{{J_1}^2(\eta)}{\eta\sqrt{\eta^2+\mathrm{i}(r_0^2\omega/\alpha_{sub})}}$ in the integrand rapidly decreases to zero for $\eta > 10$, while for $\eta < 10$, the first term in the integrand has very little variation (<5%) and can be approximated by its value at $\eta = 0$. Equation (19) is then approximated as

$$\theta_{LED}(\omega) \approx \frac{2Q_0}{\pi k_{sub} r_0} \left[1 + \sqrt{\frac{k_{encap} c_{encap} \rho_{encap}}{k_{sub} c_{sub} \rho_{sub}}} \tanh\left(h_{encap} \sqrt{\mathrm{i}\omega/\alpha_{encap}} \right) \right]^{-1} \int_0^\infty \frac{{J_1}^2(\eta)}{\eta\sqrt{\eta^2 + \mathrm{i}(r_0^2\omega/\alpha_{sub})}} \mathrm{d}\eta. \tag{20}$$

Here $\sqrt{\omega/\alpha_{encap}}$ is usually larger than, or on the order of, a few μm^{-1} for polymer with period less than 1 ms as in applications of optogenetics[26] and high power LEDs.[27] For h_{encap} larger than, on the order of, a few μm (e.g., 7 μm in Fig. 1), $\tanh(h_{encap}\sqrt{\mathrm{i}\omega/\alpha_{encap}}) \approx 1$ such that the above equation becomes

$$\left[1 + \sqrt{\frac{k_{encap} c_{encap} \rho_{encap}}{k_{sub} c_{sub} \rho_{sub}}} \right] \frac{\pi k_{sub} r_0}{Q_0} \theta_{LED}(\omega) \approx 2 \int_0^\infty \frac{{J_1}^2(\eta)}{\eta\sqrt{\eta^2 + \mathrm{i}(r_0^2\omega/\alpha_{sub})}} \mathrm{d}\eta = \frac{\sqrt{\mathrm{i}r_0^2\omega/\alpha_{sub}} - J_1(2\sqrt{\mathrm{i}r_0^2\omega/\alpha_{sub}}) + L_1(2\sqrt{\mathrm{i}r_0^2\omega/\alpha_{sub}})}{\mathrm{i}r_0^2\omega/\alpha_{sub}}, \tag{21}$$

where L_1 is the 1st-order modified Struve function.[25] The left hand side of Eq. (21) is the normalized temperature increase, while the right hand side depends only on $r_0^2\omega/\alpha_{sub}$, which can be related to the μ-ILED area πr_0^2 and pulse period t_0

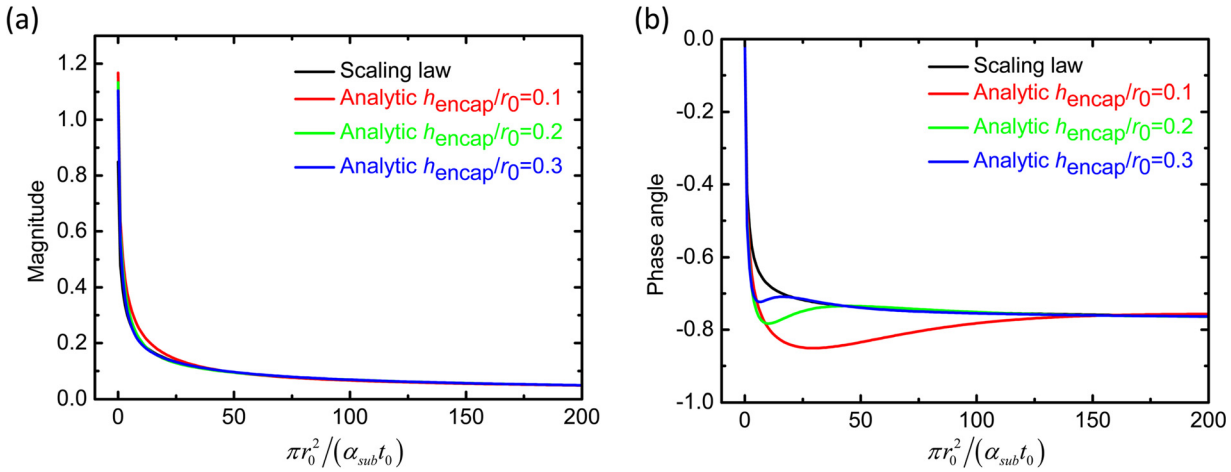

FIG. 5. The normalized μ-ILED temperature increase in (a) magnitude and (b) phase angle due to a sinusoidal power.

by $r_0^2\omega/\alpha_{sub} = 2(\pi r_0^2)/(\alpha_{sub}t_0)$. For $\omega = 0$, the right hand side of Eq. (21) is $8/(3\pi)$. Equation (21) gives a simple scaling law for the temperature increase, and is shown in Figs. 5(a) and 5(b) for the magnitude and phase angle of $\left[1+\sqrt{\frac{k_{encap}c_{encap}\rho_{encap}}{k_{sub}c_{sub}\rho_{sub}}}\right]\frac{\pi k_{sub}r_0}{Q_0}\theta_{LED}(\omega)$ in Eq. (21) versus $\pi r_0^2/(\alpha_{sub}t_0)$, which is a dimensionless combination of μ-ILED area, substrate thermal diffusivity α_{sub}, and pulse period t_0. As $\pi r_0^2/(\alpha_{sub}t_0)$ increases, the magnitude decreases from $8/(3\pi)$ to 0, and the phase angle decreases from 0 to $-\pi/4$. The analytic solution (16) also shown in Fig. 5 for the material parameters described in Sec. II B and $h_{encap}/r_0 =$ 0.1, 0.2, and 0.3, agree well with the scaling law for relatively large $\pi r_0^2/(\alpha_{sub}t_0)$.

B. A scaling law for temperature increase due to a pulsed power

For a pulsed power (Fig. 1(c)) given in Eq. (6), the scaling law for the temperature increase of μ-ILED is obtained from Eq. (21) via the method of superposition as

$$\left[1+\sqrt{\frac{k_{encap}c_{encap}\rho_{encap}}{k_{sub}c_{sub}\rho_{sub}}}\right]\frac{\pi k_{sub}r_0}{Q_0}\Delta T_{LED}(t;\omega) \approx \frac{8D}{3\pi} + \sum_{n=1}^{\infty}\left|\frac{\sqrt{\mathrm{i}r_0^2 n\omega/\alpha_{sub}} - J_1(2\sqrt{\mathrm{i}r_0^2 n\omega/\alpha_{sub}}) + L_1(2\sqrt{\mathrm{i}r_0^2 n\omega/\alpha_{sub}})}{\mathrm{i}r_0^2 n\omega/\alpha_{sub}}\right| \times \left[\begin{array}{c}\frac{\sin(2n\pi D)}{n\pi}\cos(n\omega t+\delta_n)\\ +\frac{1-\cos(2n\pi D)}{n\pi}\sin(n\omega t+\delta_n)\end{array}\right], \quad (22)$$

where δ_n is the phase angle of $[\sqrt{\mathrm{i}r_0^2\omega/\alpha_{sub}} - J_1(2\sqrt{\mathrm{i}r_0^2\omega/\alpha_{sub}}) + L_1(2\sqrt{\mathrm{i}r_0^2\omega/\alpha_{sub}})]/(\mathrm{i}r_0^2\omega/\alpha_{sub})$. The left hand side of Eq. (22) is the normalized temperature increase of μ-ILED, which depends on the normalized time t/t_0, duty cycle D, and $\pi r_0^2/(\alpha_{sub}t_0)$. The maximum temperature increase (with respect to time) $\Delta T_{LED}^{\max}$, obtained numerically from Eqs. (21), depends only on D and $\pi r_0^2/(\alpha_{sub}t_0)$ and is shown versus D in Fig. 6 for $\pi r_0^2/(\alpha_{sub}t_0) = 5$, 50, and 500. It is clearly observed that small duty cycle D or large $\pi r_0^2/(\alpha_{sub}t_0)$ are most effective to reduce the maximum temperature increase. For large $\pi r_0^2/(\alpha_{sub}t_0) \gg 1$, the maximum temperature increase in LED is approximately linear with respect to the duty cycle D, and is given by

$$\Delta T_{LED}^{\max} \approx \frac{0.48Q_0}{k_{sub}\sqrt{\pi r_0^2}}\frac{D}{1+\sqrt{\frac{k_{encap}c_{encap}\rho_{encap}}{k_{sub}c_{sub}\rho_{sub}}}} \quad \text{for} \quad \frac{\pi r_0^2}{\alpha_{sub}t_0} \gg 1, \quad (23)$$

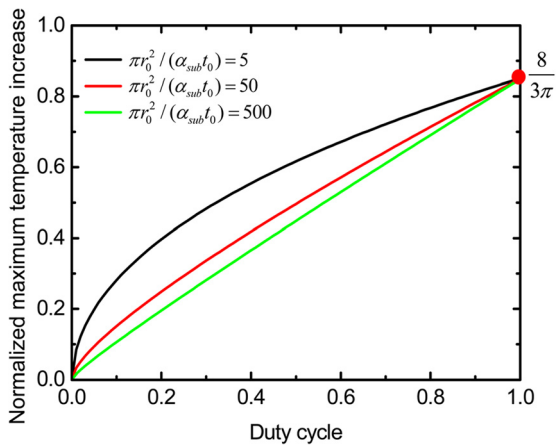

FIG. 6. The normalized maximum μ-ILED temperature increase for the pulsed power versus duty cycle.

where πr_0^2 is the in-plane area of μ-ILED. These results may serve as guidelines for the thermal management design of μ-ILED.

IV. CONCLUSIONS

We have developed an analytic model, validated by 3D FEA and experiments, to study the thermal properties of μ-ILED in a pulsed operation. A simple scaling law for the μ-ILED temperature after saturation shows that the normalized maximum temperature increase depends only on two non-dimensional parameters: duty cycle D, and $\pi r_0^2/(\alpha_{sub} t_0)$, where πr_0^2 is in-plane area of μ-ILED, α_{sub} is the thermal diffusivity of the substrate, and t_0 is the period of the pulse. Large $\pi r_0^2/(\alpha_{sub} t_0)$ or small D is effective to dissipate heat and therefore reduce the temperature. For relative large $\pi r_0^2/(\alpha_{sub} t_0)$, a simple, analytic formula for the maximum temperature increase is obtained, which shows a linear proportionality to the duty cycle D. These provide useful design guidelines for avoiding adverse heating of μ-ILED.

ACKNOWLEDGMENTS

J.S. acknowledges the support from the Provost Award from the University of Miami. C.L. acknowledges the support from the NSFC (Grant No. 11172263) and the New Star Program from Zhejiang University. Y.H. acknowledges the supports from NSF and NSFC.

[1]J. Y. Tsao, M. E. Coltrin, M. H. Crawford, and J. A. Simmons, Proc. IEEE **98**, 1162 (2010).
[2]E. F. Schubert and J. K. Kim, Science **308**, 1274 (2005).
[3]T. I. Kim, Y. H. Jung, J. Song, D. Kim, Y. Li, H. S. Kim, I. S. Song, J. J. Wierer, H. A. Pao, Y. Huang, and J. A. Rogers, Small **8**, 1643 (2012).
[4]R. M. Gagliardi and S. Karp, *Optical Communications* (Wiley-Interscience, New York, 1976).
[5]M. E. Llewellyn, K. R. Thompson, K. Deisseroth, and S. L. Delp, Nat. Med. **16**, 1161 (2010).
[6]H. S. Kim, E. Bruechner, J. Song, Y. Li, S. Kim, C. Lü, J. Sulkin, K. Choquette, Y. Huang, R. G. Nuzzo, and J. A. Rogers, Proc. Natl. Acad. Sci. U.S.A. **108**, 10072 (2011).
[7]C. Lü, Y. Li, J. Song, H. S. Kim, E. Bruechner, B. Fang, K. C. Hwang, Y. Huang, R. G. Nuzzo, and J. A. Rogers, Proc. R. Soc. A **468**, 3215 (2012).
[8]L. Yang, J. Hu, and M. W. Shin, IEEE Electron Device Lett. **29**, 863 (2008).
[9]Y. Yu, T. Y. Tom Lee, and V. A. Chiriac, IEEE Trans. Compon. Packag. Technol. **2**, 1172 (2012).
[10]V. Kyyhkynen, J. Valtanen, and E. Ristolainen, IEEE Trans. Compon. Packag. Technol. **27**, 117 (2004).
[11]D. Schweitzer, IEEE Trans. Compon. Packag. Technol. **32**, 478 (2009).
[12]J. Palacín, M. Salleras, J. Samitier, and S. Marco, IEEE Trans. Adv. Packag. **28**, 694 (2005).
[13]Z. Vaitonis, A. Stonkus, and A. Zukauskas, IET Optoelectron. **6**, 52 (2012).
[14]S. Pal and H. Xie, J. Micromech. Microeng. **19**, 065007 (2009).
[15]V. Székely and M. Rencz, IEEE Trans. Compon. Packag. Technol. **23**, 587 (2000).
[16]M. Janicki, J. Banaszczyk, B. Vermeersch, G. D. Mey, and A. Napieralski, Microelectron. Reliab. **51**, 1351 (2011).
[17]L. Yang, S. Jang, W. Hwang, and M. Shin, Thermochim. Acta **455**, 95 (2007).
[18]Z. Hu, B. Carlberg, C. Yue, X. Guo, and J. Liu, in *International Conference on Electronic Packaging Technology and High Density Packaging* (2009), pp. 481–484.
[19]A. P. Dhorajiya, M. S. Mayeed, G. W. Auner, R. J. Baird, G. M. Newaz, R. Patwa, and H. Herfurth, ASME J. Eng. Mater. Technol. **132**, 011004 (2010).
[20]O. Andersson and G. P. Johari, J. Chem. Phys. **134**, 124903 (2011).
[21]N. S. Satarkar, S. A. Meenach, K. W. Anderson, and J. Z. Hilt, AiChE J. **57**, 852 (2011).
[22]R. Li, Y. Li, C. Lü, J. Song, R. Saeidpouraza, B. Fang, Y. Zhong, P. M. Ferreira, J. A. Rogers, and Y. Huang, Soft Matter **8**, 7122 (2012).
[23]B. Solano, S. Rolt, and D. Wood, Proc. Inst. Mech. Eng. C: J. Mech. Eng. Sci. **222**, 73 (2008).
[24]ABAQUS Analysis User's Manual V6.9, Dassault Systèmes, Pawtucket, 2009.
[25]R. M. Aarts and A. J. E. M. Janssen, J. Acoust. Soc. Am. **113**, 2635 (2003).
[26]N. Li, J. E. Downey, A. B. Shir, A. A. Gilad, P. Walczak, H. Kim, S. E. Joel, J. J. Pekar, N. V. Thakor, and G. Pelled, Proc. Natl. Acad. Sci. U.S.A. **108**, 8838 (2011).
[27]C. Willert, B. Stasicki, J. Klinner, and S. Moessner, Meas. Sci. Technol. **21**, 075402 (2010).